Highly Graphitic Carbon Coating on $Li_{1.25}Nb_{0.25}V_{0.5}O_2$ Derived from Precursor with Perylene Core for High-power Battery Applications

Ruijie Qi,[†] Itsuki Konuma,[†] Benoît D.L. Campéon,[∇] Yuko Kaneda,[#] Masashi Kondo,[#] and Naoaki Yabuuchi[∇,†,‡,]*

†Department of Chemistry and Life Science, Yokohama National University, 79-5 Tokiwadai, Hodogaya-ku, Yokohama, Kanagawa 240-8501, Japan

∇Advanced Chemical Energy Research Center, Yokohama National University, 79-5 Tokiwadai, Hodogaya-ku, Yokohama, Kanagawa 240-8501, Japan

#Instrumental Analysis Center at Yokohama National, Yokohama National University, 79-5 Tokiwadai, Hodogaya-ku, Yokohama, Kanagawa 240-8501, Japan

‡Elements Strategy Initiative for Catalysts and Batteries, Kyoto University, f1-30 Goryo-Ohara, Nishikyo-ku, Kyoto 615-8245, Japan

ABSTRACT

A Li-excess cation-disordered rocksalt positive electrode material with Nb/V ions, $Li_{1.25}Nb_{0.25}V_{0.5}O_2$ (LNVO), delivers a high reversible specific capacity of >250 mA h g^{-1} on the basis of two-electron redox of V^{3+}/V^{5+}. However, the inferior rate performance originating from a character of the disordered structure prevents its use for practical applications. Here, a facile and efficient top-down approach to synthesize nanosized LNVO carbon composited materials has been developed through a combination of ball-milling and subsequent heat-treating steps. The markedly improved rate capability is achieved by highly graphitic carbon coating with superior conductivity derived from a precursor with a perylene core. The growth of particle sizes of LNVO is effectively suppressed by uniform mixing of the precursor by optimized milling conditions. The optimized nanosized sample with shorter Li ion migration paths shows excellent rate capability for the rocksalt oxide. Moreover, superior capacity retention for continuous 100 cycles is also achieved. Furthermore, by lowering Li ion migration barrier at elevated temperatures, a larger reversible specific capacity of 300 mA h g^{-1}, which nearly corresponds to its theoretical specific capacity, is obtained, coupled with further improved rate capability because of facile conduction for Li ions in oxides and electrolyte. This finding opens the possibility to develop high performance electrode materials with cation-disordered rocksalt structure for practical battery applications.

INTRODUCTION

Facing the increasing threat of global climate change, the market of electric vehicles equipped with rechargeable Li-ion batteries (LIBs) as power sources is rapidly increasing to reduce dependence on fossil fuels. Electrochemical properties of LIBs are restricted by positive electrode materials, and thus advanced positive electrode materials with higher energy and power density are desired.[1-4] Increasing attention has been focused on Li-excess cation-disordered rocksalt (DRS) oxides over the last couple of years due to their higher capacity and wider variety of chemistry than present cobalt-/nickel-based oxides with a layered structure,[5,6] leading to a beneficial advantage on the further development of LIBs. Unlike the ordered layered oxides which have a two-dimensional network for Li migration paths enabling high power applications,[7] DRS oxides have been considered electrochemically inactive for a long time, because there is a less obvious migration path for Li ion associated with the statistical distribution of cationic species. Although recent research has shown the feasibility of macroscopic percolating networks for Li ion in DRS oxides under Li-excess condition,[8] the relatively larger Li ion migration barriers of DRS oxides when compared with the layered oxide still restricts its electrode performance at a high rate condition.

Much effort has been spent on addressing the kinetic issue of LIBs such as optimization of chemical compositions, surface modification, nanosizing, and the preparation of carbon composited materials.[9-13] Among them, nanosizing and carbon coating are widely adopted owing to their simplicity and universality. In this study, a Nb-V binary oxide, $Li_{1.25}Nb_{0.25}V_{0.5}O_2$ (LNVO) with the DRS structure, which is found in $x = 0.33$ in $x\ Li_3NbO_4 - (1-x)\ LiVO_2$ binary system, is targeted as a model system.[14] Carbon composited LNVO delivers a high specific capacity of >250 mA h g^{-1} which is solely based on cationic redox of V^{3+}/V^{5+}. However, at higher specific current

density, its capacity dramatically drops due to the inferior electronic conductivity and the intrinsically limited Li ion migration within the percolating network in the DRS structure. To overcome these hindrances, the reduction of the electron transfer resistance and shortening of Li ion migration paths are targeted. To that end, a ball-milling method is introduced to simultaneously decrease particle size and mix the oxide with a carbon source. Initially, synthesized LNVO has large particles and then particle size of LNVO is effectively reduced through dry ball-milling process. However, as a result of nanosizing, these small particles prepared by dry ball-milling agglomerated with non-uniform dispersion of the carbon source. Therefore, an additional wet ball-milling process with ethanol is adopted to prevent the agglomeration of nanosized particles obtained by milling with better dispersion of the carbon source, leading to more uniform nanosized particles and carbon coating. As the carbon source, perylene-3,4,9,10-tetracarboxylic dianhydride (PTCDA) is selected because of the similar conjugated carbon configuration between its perylene core and graphite, which eases its conversion into highly graphitic carbon with superior electronic conductivity during the subsequent heat-treating.[15] By applying such the top-down synthesis approach, nanostructured and carbon coated LNVO with the DRS structure is synthesized. Moreover, well optimized LNVO with the DRS structure shows good cyclability and excellent rate-capability which are competitive with layered materials used for commercial battery applications. From these results, the feasibility of the V-based Li-excess oxides with the DRS structure as electrode materials for battery applications is evaluated in detail.

EXPERIMENTAL

Synthesis of Material: $Li_{1.25}Nb_{0.25}V_{0.5}O_2$ (LNVO) was prepared by a solid-state reaction from Li_2CO_3 (98.5%, Kanto Kagaku), Nb_2O_5 (99.9%, Wako Pure Chemical Industries), and V_2O_3 (98%, Sigma-Aldrich Japan). The precursors were mixed thoroughly by wet ball-milling at 300 rpm with ethanol for 5 h and the mixtures were pressed into pellets after drying in air. The pellets were heated at 950 °C for 12 h in an argon atmosphere. Thereafter, as-prepared LNVO was stored in an Ar-filled glovebox. The carbon coated LNVO samples with different particle sizes were synthesized by a ball-milling method. LNVO (0.8 g) and PTCDA (0.161 g) or sucrose (0.192 g) were mixed using a mortar and a pestle, and the mixture was then ball-milled by different conditions. The targeted sample labeled "1-Dry" was synthesized from a mixture of LNVO and PTCDA by dry milling at 300 rpm for a total of 36 h without solvent. The mixture was taken out from the container every 12 h and mixed with a mortar and a pestle to ensure sample uniformity during the milling process. "2-Wet" was synthesized at 300 rpm for a total of 36 h with ethanol. "3-Dry&Wet" was synthesized at 300 rpm for 24 h by dry milling followed by wet milling for 12 h with ethanol. For comparison, sucrose was also used as the carbon source and milled with the same condition of "3-Dry&Wet" sample. After milling with the carbon source, the samples were finally calcinated at 700 °C for 4 h under Ar atmosphere.

Electrochemistry: Electrode performance of the samples was examined in two-electrode type cells (TJ-AC, Tomcell Japan) and three-electrode type cells (TR-DM, Tomcell Japan). The electrolyte consisted of 1.0 mol dm^{-3} $LiPF_6$ dissolved in ethylene carbonate/dimethyl carbonate (1:1 by volume) (Kishida Chemical). The carbon composited positive electrodes consisting of 80 wt% active material (including 3.7 wt% coated carbon), 10 wt% acetylene black, and 10 wt% poly(vinylidene fluoride), was pasted on an aluminum foil. The electrode slurry was dried under vacuum and further heated at 120 °C in vacuum. Metallic lithium (Honjo Metal) and pre-lithiated

graphite, which was prepared via direct contact of the fresh graphite (Wako Pure Chemical Industries) and lithium metal foil in the presence of above $LiPF_6$ based electrolyte, were used as the negative electrodes.[16,17] The capacity of graphite is normalized to 1.5 times larger than the capacity of LNVO. Li cells were assembled in an Ar-filled glovebox. The cells were cycled at a specific current density ranging from 10 mA g^{-1} to 2560 mA g^{-1} at room temperature and 50 °C. Electrochemical impedance spectra (EIS) were carried out by using a potentiostat equipped with a frequency response analyzer (SP-200, Bio-Logic).

Characterization of Samples: Particle morphology of the samples was observed using a scanning electron microscope (SEM, JCM-6000, JEOL) with an acceleration voltage of 15 kV. X-ray diffraction (XRD) patterns of the samples were collected using an X-ray diffractometer (D2 PHASER, Bruker Corp. Ltd.) equipped with a one-dimensional X-ray detector using Cu Kα radiation generated at 300 W (30 kV and 10 mA) with a Ni filter. Synchrotron XRD data were collected at the beamline BL16B2 in SPring-8 synchrotron facility in Japan. The measurement was conducted using an automatic powder diffraction system for Debye–Scherrer geometry using a capillary sample. The wavelength of X-rays was calibrated to be 0.500 Å. Structural refinement analysis was carried out using GSAS software with EXPGUI interface.[18,19] *In-situ* XRD data were collected by a battery cell equipped with a Be window combined with an X-ray diffractometer (D8 ADVANCE; Bruker Corp., Ltd.). Nonmonochromatized Cu Kα (1.5406 - 1.5444 Å) radiation with a Ni filter as an X-ray source and a diffractometer with a Bragg-Brentano geometry were utilized. The Brunauer-Emmett-Teller (BET) specific surface area was measured at 77 K on a micromeritics surface area and porosity analyzer (BELSORP-MINI X; Microtrac MRB). The graphitization degree of the coating carbon was investigated with a Raman spectroscopy (inVia reflex from RENISHaW) and transmission electron microscopy (TEM) (JEM-2100F) operated under 200 kV.

The thermal stability of electrode materials was evaluated by differential scanning calorimetry (DSC, DSC-60 Plus, SHIMADZU) with a high pressure-resistant container made of stainless steel. 0.75 μL of electrolyte was added to 2.5 mg of samples. Containers were heated at 10 °C min^{-1} in nitrogen atmosphere from 25 to 400 °C. Hard X-ray absorption spectroscopy (XAS) at V K-edge was performed at beamline BL-12C of the Photon Factory Synchrotron Source in Japan. The hard XAS spectra were obtained with a silicon monochromator in a transmission mode. The intensity of the incident and transmitted X-ray was measured using an ionization chamber at room temperature. The composite electrodes were rinsed with dimethyl carbonate and sealed in a water-resistant polymer film in the Ar-filled glovebox. XAS spectra was normalized using the program, IFEFFIT.[20] A cubic spline procedure was utilized for the estimation of post-edge background.

RESULTS AND DISCUSSION

Synthesis of Carbon Coated $Li_{1.25}Nb_{0.25}V_{0.5}O_2$ with Different Particle Sizes. An XRD pattern of as-prepared LNVO is shown in **Supporting Figure S1a**. The materials crystallize into a partially cation-ordered layered phase as visualized by the presence of the diffraction line at 18°, which is indexed to 111 diffraction line with a cubic symmetry.[14,21] This peak can be assigned to 003 diffraction line for α-$NaFeO_2$-type layered structure with rhombohedral symmetry, but a crystallographic symmetry changes to cubic symmetry when a ratio of $c_{hex.}/a_{hex.}$ lattice parameters is close to 4.9.[22] The non-uniform particle size ranging from 10 to 100 μm is shown in **Supporting Figure S1b**. It is noted that as-prepared sample shows inferior electrochemical performance (**Supporting Figure S1b**) because of excessive growth of particle size on heating at higher temperatures. In addition, the rearrangement of vanadium ions in the cubic-close-packed oxide lattice on charge results in the loss of ordered structure.[23] The detailed structural evolution of

LNVO will be discussed in the later section by *in-situ* XRD study. Although the percolating network enables the migration of Li ion in the disordered structure,[8] the intrinsic inferior electrode kinetics related to low ionic conductivity of DRS materials than layered materials restricts facile Li ion migration, and this problem turns into a critical problem in samples with large particle size. Reduction of particle size coupled with the suppression of particle growth by carbon coating is therefore expected to be an effective strategy to overcome these drawbacks by shortening Li ion migration length assisted with an increase in electronic conductivity.[24,25]

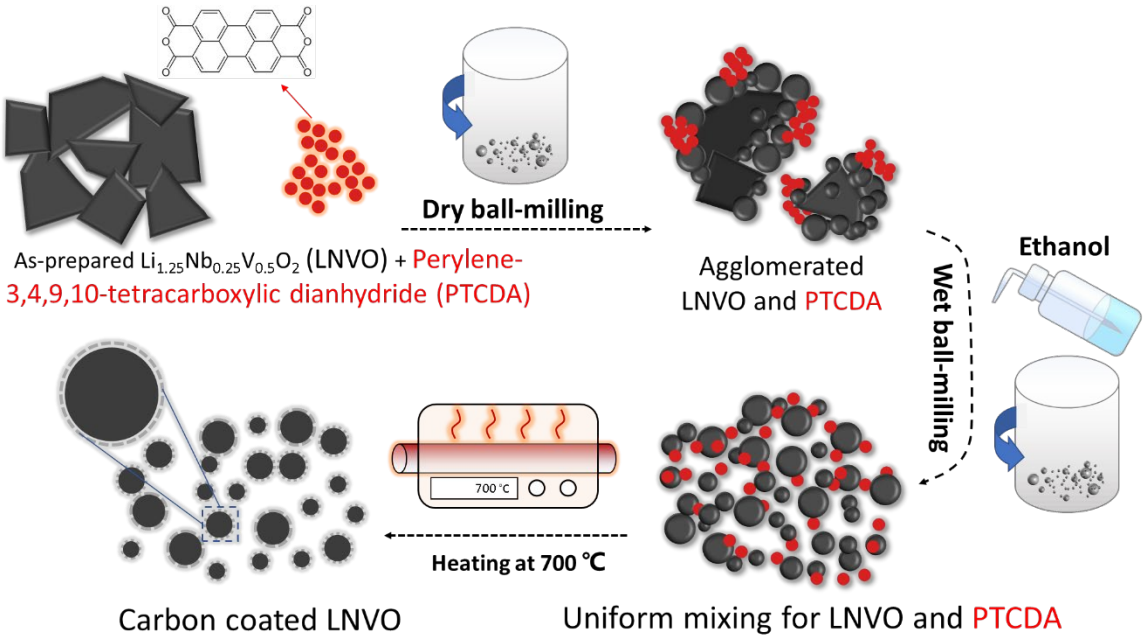

Figure 1. A schematic illustration of the synthesis of nanostructured and carbon coated $Li_{1.25}Nb_{0.25}V_{0.5}O_2$ by the top-down approach assisted with ball milling.

Three samples with different particle sizes, "1-Dry", "2-Wet", and "3-Dry&Wet", were prepared through ball-milling and heat-treating of the above as-prepared LNVO with PTCDA (see the experimental section for details and **Supporting Figure S2**). The detailed synthesis process of the

most optimized "3-Dry&Wet" sample is schematically shown in **Figure 1**. As shown in **Figure 2a**, all three samples possess the same partially cation-ordered layered structure as observed for as-prepared LNVO. Although $LiVO_2$ crystallizes into a perfectly ordered layered structure,[26] Nb ions with d^0 configuration energetically stabilize the disordered structure,[27] leading to the partial cation mixing between Li and transition metal ions (V^{3+} and Nb^{5+}) as illustrated in **Figure 2c**. Besides, after the substitution of V ions by Li/Nb ions with larger ionic radii, the presence of a shoulder is noted on the enlarged 400 diffraction line as shown in **Figure 2a**. This observation indicates non-uniform cation distributions in the sample. Indeed, nanoscale phase segregation in LNVO was demonstrated in our former study.[14] Noticeably, "3-Dry&Wet" sample has broader diffraction lines than "1-Dry" and "2-Wet" samples, indicating smaller scattering domains with lower crystallinity (**Supporting Figure S3a**). The difference in particle size is evidenced by SEM and BET measurements shown in **Figure 2b** and **Supporting Figure S3b**. The detailed specific surface area (SSA) and particle size values of the three samples are also shown in **Figure 2b** and **Supporting Figure S3c**. The result shows that the dry ball-milling approach is less effective in decreasing particle size of LNVO and mixing with PTCDA, leading to a relatively small surface area of less than 10 $m^2\ g^{-1}$. In contrast, wet milling effectively reduces particle size probably because of the suppression of agglomeration of LNVO on milling and better dispersion of PTCDA, resulting in large surface area of over 20 $m^2\ g^{-1}$. Particle size is further reduced by the combination of both methods, leading to a large surface area of ~40 $m^2\ g^{-1}$. Moreover, the least agglomeration of LNVO particles for "3-Dry&Wet" sample is observed from the SEM image. Note that a uniform distribution of O, V, and Nb ions at the nanoscale is clearly evidenced from TEM with energy dispersive X-ray spectroscopy (EDX) (**Supporting Figure S4**). All obtained carbon coated

samples are expected to contain a similar amount of carbon (approximately 4 wt%) according to a thermogravimetric curve of PTCDA as shown in **Supporting Figure S5**.

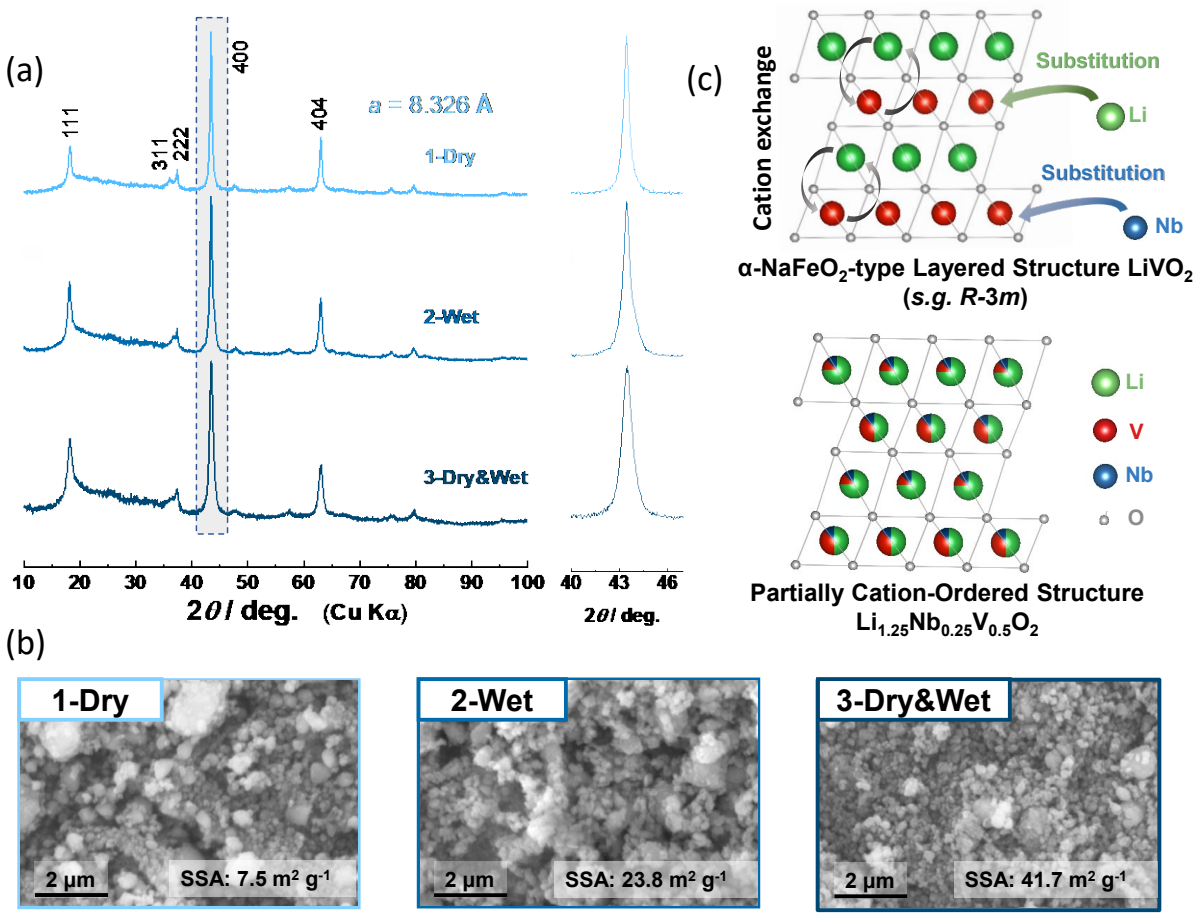

Figure 2. Structural characterization by XRD (a), SEM and BET analysis (b) of LNVO samples prepared by different conditions; "1-Dry", "2-Wet", and "3-Dry&Wet". Schematic illustrations of the crystal structure for LNVO compared with stoichiometric $LiVO_2$ are also shown in (c).

Impact of Particle Size of Carbon Coated $Li_{1.25}Nb_{0.25}V_{0.5}O_2$ on Rate Capability. The electrode performance of LNVO samples is significantly improved by the reduction of particle size and carbon coating as shown in **Figure 3**. Regardless of particle size differences, all three

samples deliver a high reversible specific capacity of over 230 mA h g^{-1} at a slow rate of 10 mA g^{-1} (**Figure 3a**), which is much larger than as-prepared LNVO which delivers less than 50 mA h g^{-1} at 10 mA g^{-1} (**Supporting Figure S1b**). Large reversible capacity proves that shortening Li ion migration length can overcome the negative effect brought by inferior electrode kinetics for the DRS oxides. At higher rates, clear differences in discharge capacities are noted for three samples. As shown in **Figure 3b and c**, although "1-Dry" sample delivers a comparable capacity with "3-Dry&Wet" sample at a slow rate of 10 mA g^{-1}, the sample with a relatively large size cannot satisfy the demand for high power battery applications. The discharge specific capacity of "1-Dry" sample is decreased to 80 mA h g^{-1} when the specific current density reaches 2560 mA g^{-1}, corresponding to a retention rate of only 35%. In contrast, "3-Dry&Wet" sample exhibits a much superior rate capability, reaching up to 69% retention rate at 2560 mA g^{-1}. Note that similar sample loading for "1-Dry" and "3-Dry&Wet" samples is used, indicating that a loading difference is not responsible for the improvement of rate capability. "2-Wet" sample also shows good rate capability, but a better result is obtained for "3-Dry&Wet" sample. This trend is further supported by EIS measurement (**Figure 3d**), which confirms the lowering of the impedance with the particle size reduction, leading to better rate capability.

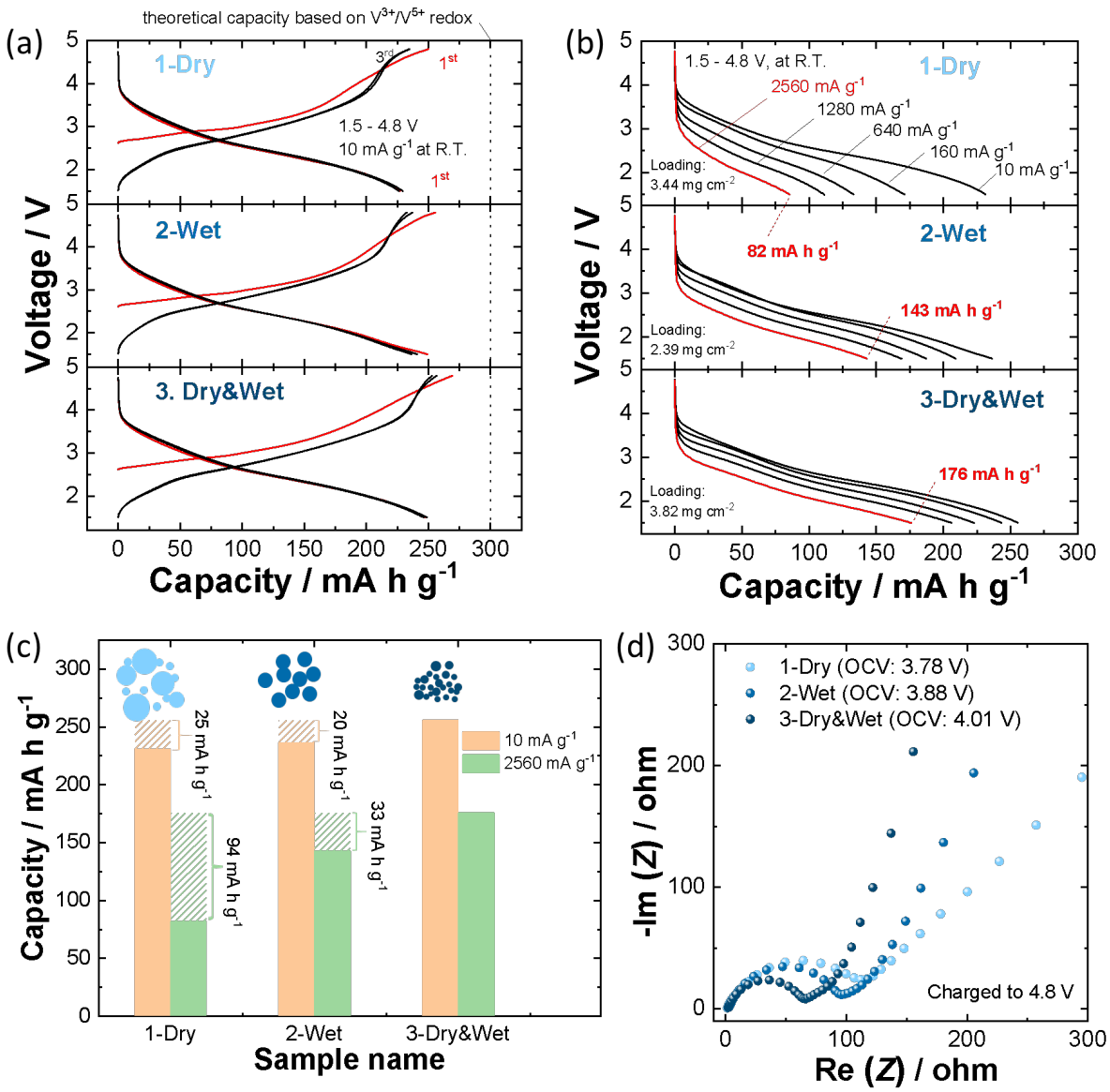

Figure 3. Comparison of electrochemical properties of LVNO with different particle size; (a) galvanostatic charge/discharge curve at 10 mA g^{-1}, (b) discharge curves with the different specific current density (10 to 2560 mA g^{-1}) after charge to 4.8 V at 100 mA g^{-1} and held at 4.8 V for 1 hour, and (c) comparison and summary of rate capability of three samples, and (d) Nyquist plots after charge to 4.8 V at 10 mA g^{-1}. Sample mass loading is also shown in (b).

Comparative study on carbon sources for nanosized and carbon coated $Li_{1.25}Nb_{0.25}V_{0.5}O_2$. In addition to nanosizing and shortening of Li migration length, the good rate capability is also originating from the highly conductive graphitic carbon coating derived from PTCDA. To further figure out the role of carbon in the rate performance of "3-Dry&Wet" sample, sucrose is utilized as a reference carbon source. Samples were prepared with PTCDA and sucrose by using the milling condition for "3-Dry&Wet" sample. A broader peak width for the 400 diffraction line is noted for the sample with sucrose as shown in **Figure 4a**, suggesting that scattering domain is smaller for the sample with sucrose. Indeed, a smaller particle size with larger surface area for the sample prepared with sucrose is found by SEM and BET analysis (**Supporting Figure S6a** and **b**). Both samples are expected to contain similar carbon contents after heating at 700 ℃ as shown in **Supporting Figure S5**. The molecular structures of PTCDA and sucrose are shown in **Figure 4a**, the conjugated carbon structure of perylene core is anticipated to be easily converted into highly conductive graphitic carbon during heat treatment compared to sucrose without conjugated carbon. This expectation is clearly demonstrated by TEM observation (**Figure 4b**) and Raman analysis (**Supporting Figure S6c**). From TEM images for both samples, a clear difference is noted for carbon structures. A non-graphitic carbon layer is observed for carbon derived from sucrose whereas a graphitic carbon layer is found for the carbon derived from PTCDA as clearly shown in **Figure 4b**. Raman study also supports this finding. The intensity ratio between the D band and G band, which corresponds to the amorphous and graphitic carbon, respectively,[28] is a good indicator to evaluate the nature of carbon. The sample with PTCDA exhibits a lower I_D/I_G ratio than the sample with sucrose, indicating a higher graphitization degree. At a low rate, both samples deliver almost the same capacities, however, the important role of graphitic carbon with high conductivity is clearly evidenced at a high rate (**Figure 4c**). Indeed, the sample with sucrose shows relatively

small discharge capacity at a high rate. It is worth noting that the superior rate capability of the sample with PTCDA is obtained with a much heavier electrode mass loading of 3.8 mg cm^{-2} than 1.7 mg cm^{-2} of the sample with sucrose. The obvious difference in impedance data is also demonstrated by EIS measurement in **Figure 4d**, and the resistance of the composite electrode, which is observed at higher to middle frequency,[29] is clearly reduced for the sample with PTCDA. The highly graphitic carbon layer is also effective to reduce the side reaction of electrolyte decomposition.[30] Consequently, the graphitic carbon layer derived from PTCDA is evidenced to play a major role in improving the rate capability of LNVO with the DRS structure.

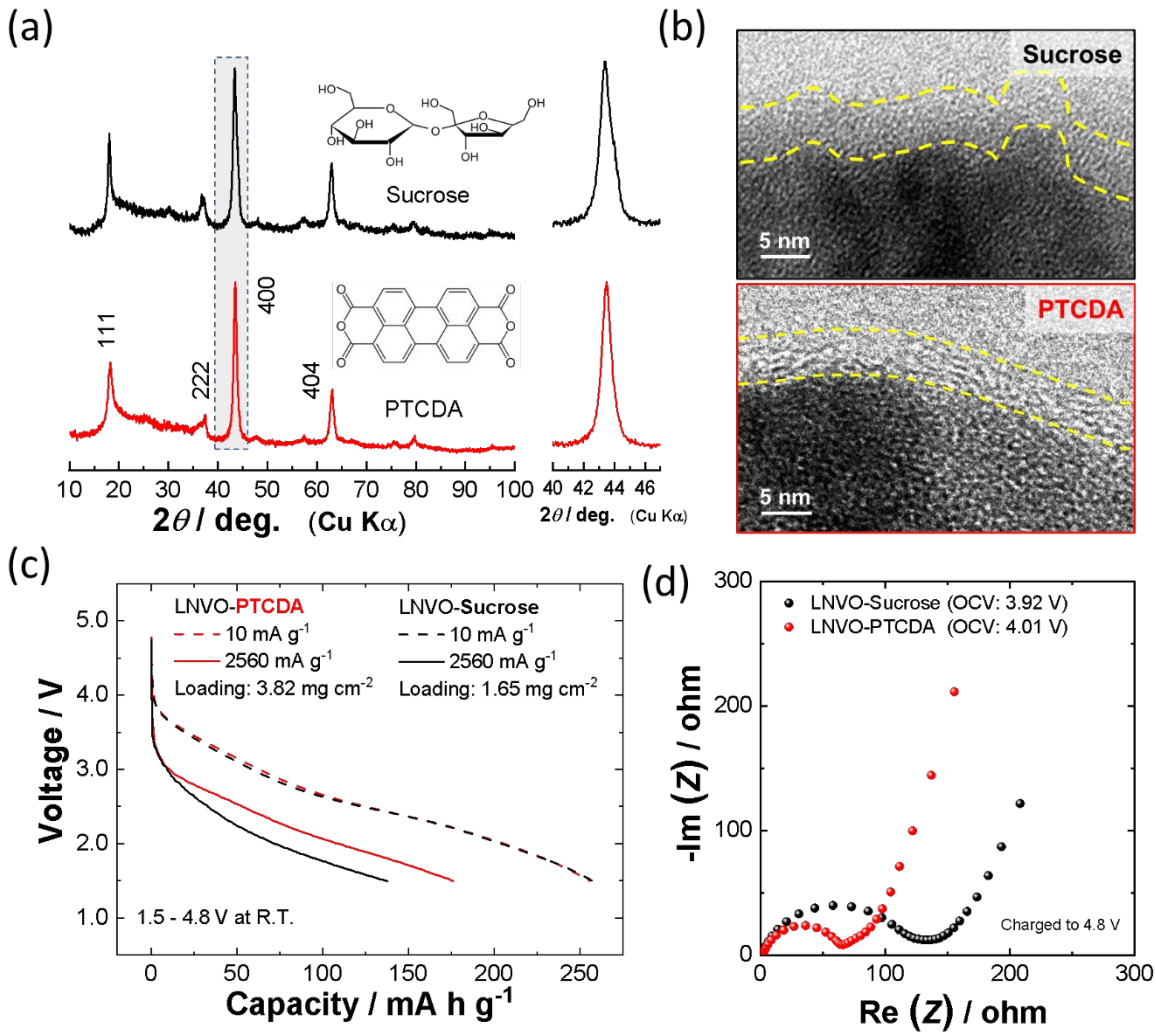

Figure 4. Characterization of LNVO sample obtained from different carbon sources, PTCDA and sucrose; (a) XRD patterns, (b) high resolution TEM images, (c) discharge curves at rates of 10 and 2560 mA g^{-1} after charged to 4.8 V at 100 mA g^{-1} and held at 4.8 V for 1 hour, and (d) EIS spectra after charged to 4.8 V. Revised

Structural evolution and thermal stability of carbon coated $Li_{1.25-x}Nb_{0.25}V_{0.5}O_2$. As shown in **Supporting Figure S7** and **Supporting Table S1**, although partial cation ordering is observed in the original crystal structure of LNVO, cation ordering is lost after initial cycle associated with

the migration character of V ions on electrochemical cycles.[14,23,31] Similar structural evolution is successfully visualized by *in-situ* XRD study for "3-Dry&Wet" LNVO sample in **Figure 5a** and **Supporting Figure S8**. The partially cation-ordered structure is retained during the initial charging ($x < 0.3$ in $Li_{1.25-x}Nb_{0.25}V_{0.5}O_2$), which is clearly evidenced from the fact that the 111 and 311 diffraction lines are visible. However, the 111 and 311 diffraction lines disappear upon further delithiation to $x = 0.5$, suggesting the structural change from the partially cation-ordered structure to DRS structure associated with the migration of V ions, leading to a more uniform site distribution of V ions in the host structure (**Figure 5b**). Besides, a decrease in the peak intensity of the DRS structure is observed upon further delithiation ($0.5 < x < 0.9$). This fact suggests that the formation of amorphous phase, and a similar finding was also reported for the Li-excess V-based oxyfluoride.[32] Moreover, peak intensity for the DRS phase is recovered upon re-lithiation, suggesting that the transition from amorphous to crystalline phase. Moreover, the diffraction lines of DRS structure located at 37.2, 43.2 and 62.8° present almost no shift during the whole charging/discharging process, indicating a small volume change. The origin of the small volume change and amorphous phase formation for V-based compounds with the DRS structure is currently under study, which will be reported in detail elsewhere.

Changes in electronic structures of V ions on electrochemical cycles were further examined by XAS study. The reversible changes in absorption energy on electrochemical cycles prove the charge compensation by V redox on the lithiation/delithiation processes in LNVO. Additionally, the increase of a pre-edge peak intensity at 5469 eV on charge is noticed (**Figure 5c**). The pre-edge peak is known to be more intensified when transition metal ions with d^0 configuration are located at tetrahedral sites.[33] This fact suggests that V^{3+} ions, originally located at the octahedral site, are oxidized to V^{5+} ions and then migrate to neighboring tetrahedral sites as shown in the

scheme of **Figure 5b**. Note that the pre-edge peak is still observed after discharge, suggesting partial occupation of V ions at tetrahedral sites after discharge.

The thermal stability of electrode materials is also important to ensure battery safety. The average operating voltage of LVNO is relatively low (mainly less than 4 V *vs.* Li/Li^+) and therefore a better thermal stability is expected when compared with Ni-based layered oxides with higher voltage.[34] DSC curves of fully charged $Li_{1-y}NiO_2$ and $Li_{1.25-y}Nb_{0.25}V_{0.5}O_2$ with electrolyte solution are compared in **Figure 5d**. The clear exothermic peak for $Li_{1-y}NiO_2$ at 200 °C indicates the chemical instability of Ni^{4+} ions whereas as for $Li_{1.25-y}Nb_{0.25}V_{0.5}O_2$, no obvious exothermic peak is observed even at 350 °C because of the superior chemical stability of V^{5+} ions. This finding suggests that safer batteries at elevated temperatures would be developed in the future employing such V-based compounds with the DRS structure.

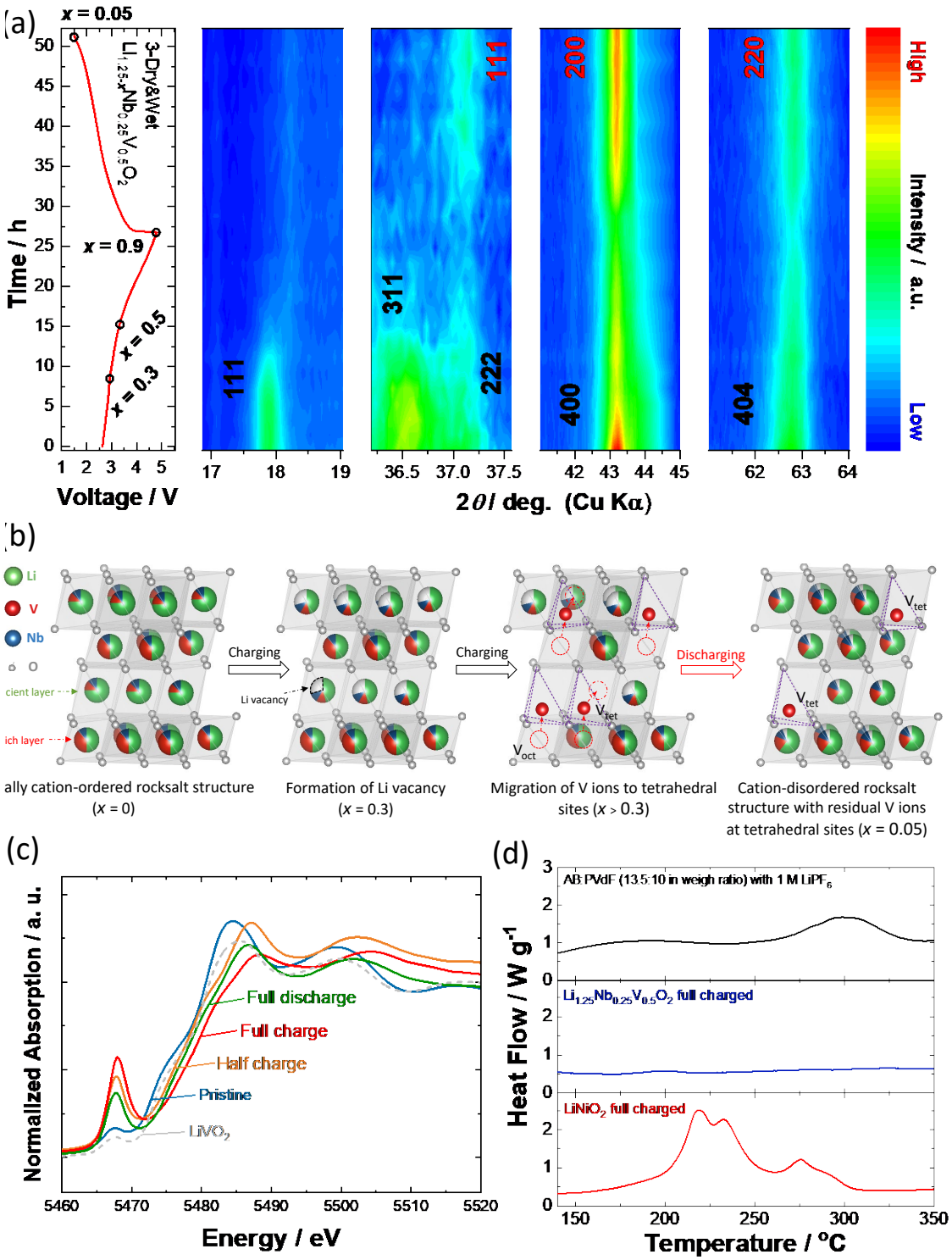

Figure 5. Reaction mechanisms of $Li_{1.25-x}Nb_{0.25}V_{0.5}O_2$: (a) a charge/discharge curve and corresponding *in-situ* XRD profile, (b) schematic illustrations of phase evolution on charge

associated with mobile V ions, (c) *ex-situ* XAS spectra on electrochemical cycles, and (d) DSC curves of the fully charged samples. Miller indices of the partially cation-ordered phase and DRS phase are described in black and red, respectively, in (a).

Feasibility of carbon coated $Li_{1.25}Nb_{0.25}V_{0.5}O_2$ as positive electrode materials for battery applications. To further examine the practical reality of LNVO, long term cyclability is tested in **Figure 6a-c**. "3-Dry&Wet" sample shows good capacity retention for the initial 30 cycles at 50 mA g^{-1}, however, the capacity degrades abruptly after 30 cycles as shown in **Figure 6a-b**. To identify the origin of degradation, the deterioration of metallic lithium negative electrode is hypothesized. To challenge this hypothesis, two approaches are utilized, (1) thicker metallic Li and (2) graphite were adopted as negative electrodes. The cyclabilities of the cells with metallic Li with 100 and 500 μm thickness are compared. As shown in **Figure 6b**, the cycling capability is significantly improved by using metallic Li with 500 μm thickness. The capacity retention is significantly increased from 40% with 100 μm Li metal to over 90% with 500 μm Li metal after 100 cycles. Besides, instead of metallic Li, by using pre-lithiated graphite as a negative electrode, good capacity retention is also obtained after 100 cycles (**Figure 6c**). Corresponding charging/discharging curves of the full-cell are also shown in the inset of the figure. These results clearly indicate that a good cyclability with LNVO is achieved by restraining the deterioration of metallic Li and demonstrate the feasibility of long cycle life for LNVO electrode materials.

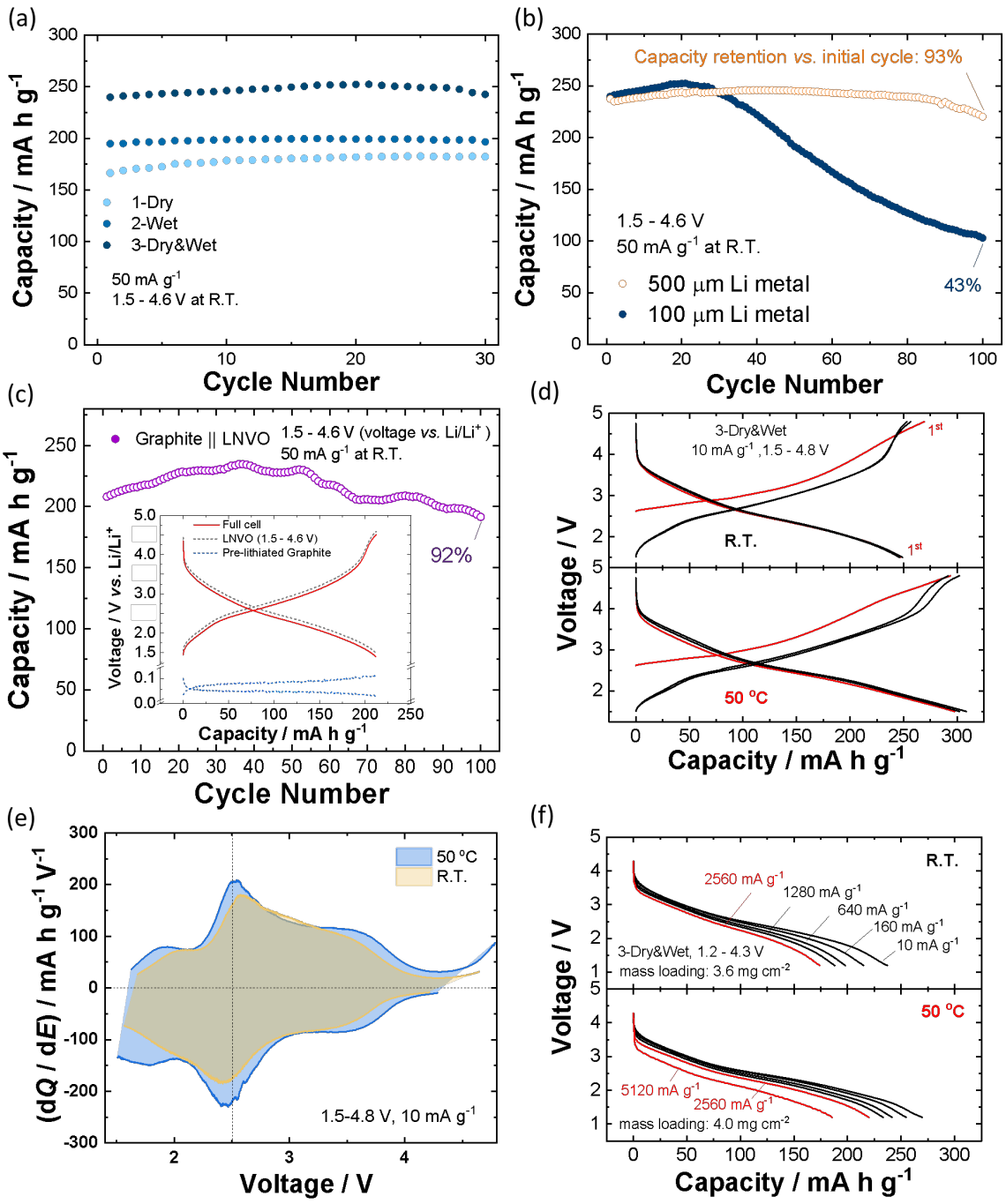

Figure 6. (a-c) Cyclability of carbon coated $Li_{1.25-x}Nb_{0.25}V_{0.5}O_2$ with different particle sizes; (a) half-cell evaluation with 100 μm Li metal, (b) comparison of half-cells assembled with different thicknesses of Li metal (100 *vs.* 500 μm). (c) a full-cell evaluation with the graphite negative electrode. (d-f) Electrochemical performances of $Li_{1.25}Nb_{0.25}V_{0.5}O_2$, "3-Dry&Wet" sample, at

elevated temperatures: (d) galvanostatic charge/discharge curves in the voltage window from 1.5 to 4.8 V, (e) corresponding differential capacity curves as a function of voltage, and (f) discharge curves at different rates after charged at 100 mA g^{-1} to 4.3 V and then held at 4.3 V for 1 h.

Electrode reversibility of carbon coated $Li_{1.25-x}Nb_{0.25}V_{0.5}O_2$ with DRS Structure at elevated temperatures. The theoretical specific capacity of LNVO reaches 300 mA h g^{-1} when reversible two-electron redox, V^{3+}/V^{5+}, is achieved. However, the observed capacities of the samples at room temperature are limited to approximately 250 mA h g^{-1} even at a slow rate of 10 mA g^{-1} regardless of particle size differences (**Figure 3a** and **c**). This observation at room temperature suggests that some of Li ion with the DRS structure are less affected by sluggish kinetics for Li ion conduction but limited by a thermodynamically controlled process. In DRS oxides, Li ion migration from the original octahedral site to the neighboring octahedral site is achieved via the occupation at the intermediate tetrahedral site, which shares faces with both original and neighboring octahedral sites. The accessible Li contents are influenced by the local configurations at the intermediate tetrahedral site.[35] When the intermediate site shares faces with only Li ion (*i.e.*, 0-TM channels), repulsive electrostatic interaction at the intermediate site is minimized, and thus Li ion pass through the tetrahedral site with a lower migration barrier by forming the percolative network for tetrahedral sites with 0-TM channels. Nevertheless, the possibility of Li migration with higher migration barriers is increased at elevated temperatures, and reversible capacities can be further enhanced. Indeed at 50 °C, "3-Dry&Wet" sample delivers a reversible specific capacity of approximately 300 mA h g^{-1}, as reported in **Figure 6d**, indicating more available Li ion are involved in the charge/discharge process, leading to the full utilization of V^{3+}/V^{5+} two-electron redox. As shown in **Figure 6e**, dQ/dE curves for "3-Dry&Wet" sample at room temperature (R.T.) and 50 °C clearly show that Li ion at the higher voltage region (3.5 – 4.0 V) are easily accessible

at elevated temperatures, resulting in higher operating voltage as electrode materials. However, improvement of rate capability is not evidenced at elevated temperatures as shown in **Supporting Figure S9a** when 4.8 V cut-off is used, which would be attributed to the accelerated chemical instability of positive electrodes coupled with the side reactions with the electrolyte solution. The deterioration of electrode performance with higher cut-off voltage is promoted at higher temperature as shown in **Supporting Figure S9b** and **c**. To avoid these problems at high voltage, the rate performances with a lower cutoff voltage of 4.3 V were tested at R.T. and 50 °C, as shown in **Figure 6f**. As expected, thanks to the better Li ion conduction in the oxide and electrolyte at 50 °C, "3-Dry&Wet" sample delivers a larger reversible capacity and excellent rate capability. Indeed, a discharge specific capacity of 185 mA h g^{-1} is obtained even at a rate of 5120 mA g^{-1}, corresponding to a discharging time of approximately 2 minutes, without using lower specific sample loading (< 1 mg cm^{-2}) or excessive carbon in the composite electrodes.

As shown in this article, carbon coated $Li_{1.25}Nb_{0.25}V_{0.5}O_2$ with the DRS structure shows excellent rate capability, and its performance is compared to that of other positive electrode materials with different structures reported in recent publications in **Figure 7**. When compared to the rocksalt oxyfluoride with two-electron cationic redox of Mn ions,[36] due to highly graphitic carbon coating, $Li_{1.25}Nb_{0.25}V_{0.5}O_2$ shows much better rate capability. Moreover, the improved rate capability of $Li_{1.25}Nb_{0.25}V_{0.5}O$ with the DRS structure is achieved, which is competitive with layered- and spinel-type electrode materials with the cation-ordered structures reported in recent publications.[11,36-40] Inferior electrode reversibility is effectively improved by the optimization of material design for the DRS oxides, leading to the further development of high-performance Li-ion batteries in the future.

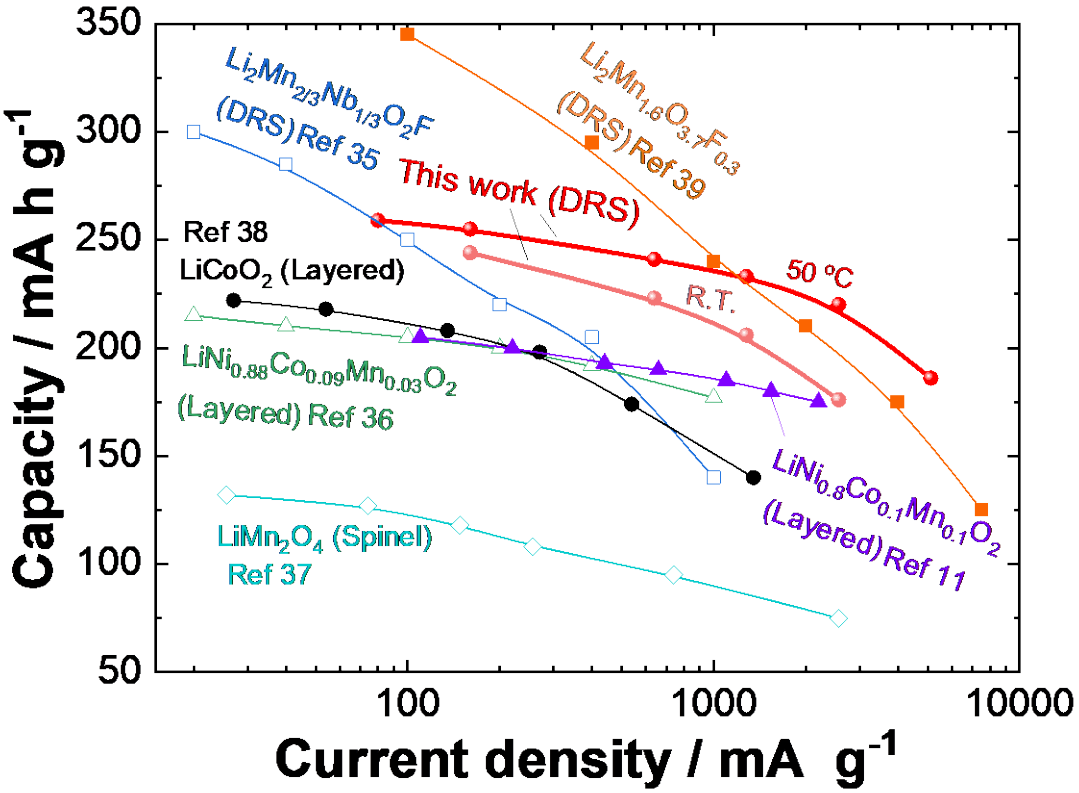

Figure 7. Comparison of the specific capacity and gravimetric current density of carbon coated $Li_{1.25}Nb_{0.25}V_{0.5}O_2$ with other positive electrode materials with different structures reported in the recent publications.[11,36-40]

CONCLUSION

The rate capability of DRS oxides is jointly controlled by Li ion migration length in percolating network and electronic conductivity. In this study, nanosized $Li_{1.25}Nb_{0.25}V_{0.5}O_2$ coated by highly graphitic carbon converted from the perylene core enables a high reversible specific capacity of >250 mA h g^{-1} which corresponds to 80% of the theoretical capacity with excellent rate capability. Additionally, an elevated temperature condition is adopted to further lower the Li ion migration barrier and activate more Li ion, which are thermodynamically inactive at lower temperature. At

elevated temperature, the lower Li ion migration barrier coupled with higher electrolyte Li ion conductivity results in full utilization of V^{3+}/V^{5+} redox and unlocks the theoretical specific capacity of 300 mA h g^{-1}. Moreover, excellent rate capability, 185 mA h g^{-1} at 5120 mA g^{-1}, is achieved with the oxide possessing the DRS structure. Because of the metastable character, DRS oxides/oxyfluorides are generally synthesized by high-energy mechanical milling, and post-annealing with carbon sources at higher temperatures results in phase segregation to thermodynamically stable phases. In contrast, $Li_{1.25}Nb_{0.25}V_{0.5}O_2$ is the thermodynamically stable phase, and therefore versatile material design with different approaches is possible as shown in this study. The results provide some insights for the further development of DRS oxides, which are competitive with commercially available layered materials, as positive electrodes for high-energy and high-power battery applications in the future.

ASSOCIATED CONTENT

Supporting Information

The Supporting Information is available free of charge at https://pubs.acs.org/doi/###

Crystallographic parameters obtained by Rietveld analysis for $Li_{1.25}Nb_{0.25}V_{0.5}O_2$ (3-Dry&Wet sample), XRD profile, electrochemical performance, and SEM image of as-prepared $Li_{1.25}Nb_{0.25}V_{0.5}O_2$, a schematic illustration of the synthesis procedure of $Li_{1.25}Nb_{0.25}V_{0.5}O_2$ prepared by different conditions, enlarged XRD profiles, BET specific surface area measurement, particle size distributions, and TEM and EDX measurement of $Li_{1.25}Nb_{0.25}V_{0.5}O_2$ (3-Dry&Wet sample), thermal gravimetric curves of carbon sources in argon atmosphere. sucrose and PTCDA; SEM and Raman spectra of $Li_{1.25}Nb_{0.25}V_{0.5}O_2$ with different carbon sources, A fitting result by Rietveld analysis for 3-Dry&Wet sample, *in-situ* XRD patterns of $Li_{1.25}Nb_{0.25}V_{0.5}O_2$ (3-Dry&Wet

sample) on electrochemical cycles; galvanostatic charge/discharge curves and results of impedance measurements for $Li_{1.25}Nb_{0.25}V_{0.5}O_2$ (3-Dry&Wet sample) at elevated temperatures.

AUTHOR INFORMATION

Corresponding Author

*Naoaki Yabuuchi

orcid.org/0000-0002-9404-5693

E-mail: yabuuchi-naoaki-pw@ynu.ac.jp

Notes

The authors declare no competing interest.

ACKNOWLEDGMENT

NY acknowledges the partial support from JSPS, Grant-in-Aid for Scientific Research (Grant Numbers 15H05701, 19H05816, and 21H04698), and MEXT program "Elements Strategy Initiative to Form Core Research Center (JPMXP0112101003)", MEXT; Ministry of Education Culture, Sports, Science and Technology, Japan. NY also thanks CBMM for the partial financial support. The synchrotron X-ray absorption work was done under the approval of the Photon Factory Program Advisory Committee (Proposal No. 2021G039). The synchrotron radiation experiments were performed at the BL19B2 of SPring-8 with the approval of the Japan Synchrotron Radiation Research Institute (JASRI) (Proposal No. 2021B1722).

ABBREVIATIONS

$Li_{1.25}Nb_{0.25}V_{0.5}O_2$ (LNVO), lithium-ion batteries (LIBs), disordered rocksalt (DRS), perylene-3,4,9,10-tetracarboxylic dianhydride (PTCDA), electrochemical impedance spectrum (EIS), scanning electron microscopy (SEM), X-ray diffraction (XRD), Brunauer-Emmett-Teller (BET), transmission electron microscopy (TEM), differential scanning calorimetry (DSC), hard X-ray absorption spectroscopy (XAS), specific surface area (SSA), energy dispersive X-ray spectroscopy (EDX), transition metal (TM), room temperature (R.T.)

REFERENCES

(1) Whittingham, M. S. Ultimate Limits to Intercalation Reactions for Lithium Batteries, *Chem. Rev.* **2014**, *114*, 11414-11443.

(2) Manthiram, A. A reflection on lithium-ion battery cathode chemistry, *Nat. Commun.* **2020**, *11*, 1550.

(3) Ikeda, N.; Konuma, I.; Rajendra, H. B.; Aida, T.; Yabuuchi, N. Why is the O3 to O1 phase transition hindered in LiNiO2 on full delithiation?, *J. Mater. Chem. A* **2021**, *9*, 15963-15967.

(4) Kubota, K. Electrochemistry and Solid-State Chemistry of Layered Oxides for Li-, Na-, and K-Ion Batteries, *Electrochemistry* **2020**, *88*, 507-514.

(5) Clément, R. J.; Lun, Z.; Ceder, G. Cation-disordered rocksalt transition metal oxides and oxyfluorides for high energy lithium-ion cathodes, *Energy Environ. Sci.* **2020**, *13*, 345.

(6) Campéon, B. D. L.; Yabuuchi, N. Fundamentals of metal oxide/oxyfluoride electrodes for Li-/Na-ion batteries, *Chem. Phys. Rev.* **2021**, *2*, 041306.

(7) Mizushima, K.; Jones, P.; Wiseman, P.; Goodenough, J. B. Li_xCoO_2 (0<x<-1): A new cathode material for batteries of high energy density, *Mater. Res. Bull.* **1980**, *15*, 783-789.

(8) Lee, J.; Urban, A.; Li, X.; Su, D.; Hautier, G.; Ceder, G. Unlocking the Potential of Cation-Disordered Oxides for Rechargeable Lithium Batteries, *Science* **2014**, *343*, 519-522.

(9) Chen, Z.; Dahn, J. Reducing carbon in $LiFePO_4$/C composite electrodes to maximize specific energy, volumetric energy, and tap density, *J. Electrochem. Soc.* **2002**, *149*, A1184.

(10) Malik, R.; Burch, D.; Bazant, M.; Ceder, G. Particle size dependence of the ionic diffusivity, *Nano Lett.* **2010**, *10*, 4123-4127.

(11) Yoon, M.; Dong, Y.; Hwang, J.; Sung, J.; Cha, H.; Ahn, K.; Huang, Y.; Kang, S. J.; Li, J.; Cho, J. Reactive boride infusion stabilizes Ni-rich cathodes for lithium-ion batteries, *Nat. Energy* **2021**, *6*, 846.

(12) Kobayashi, Y.; Sawamura, M.; Kondo, S.; Harada, M.; Noda, Y.; Nakayama, M.; Kobayakawa, S.; Zhao, W.; Nakao, A.; Yasui, A.; Rajendra, H. B.; Yamanaka, K.; Ohta, T.; Yabuuchi, N. Activation and stabilization mechanisms of anionic redox for Li storage applications: Joint experimental and theoretical study on Li_2TiO_3–

$LiMnO_2$ binary system, *Mater. Today* **2020**, *37*, 43-55.

(13) Sawamura, M.; Kobayakawa, S.; Kikkawa, J.; Sharma, N.; Goonetilleke, D.; Rawal, A.; Shimada, N.; Yamamoto, K.; Yamamoto, R.; Zhou, Y.; Uchimoto, Y.; Nakanishi, K.; Mitsuhara, K.; Ohara, K.; Park, J.; Byon, H. R.; Koga, H.; Okoshi, M.; Ohta, T.; Yabuuchi, N. Nanostructured LiMnO2 with Li3PO4 Integrated at the Atomic Scale for High-Energy Electrode Materials with Reversible Anionic Redox, *ACS Cent. Sci.* **2020**, *6*, 2326-2338.

(14) Nakajima, M.; Yabuuchi, N. Lithium-Excess Cation-Disordered Rocksalt-Type Oxide with Nanoscale Phase Segregation: $Li_{1.25}Nb_{0.25}V_{0.5}O_2$, *Chem. Mater.* **2017**, *29*, 6927-6935.

(15) Song, J.; Sun, B.; Liu, H.; Ma, Z.; Chen, Z.; Shao, G.; Wang, G. Enhancement of the Rate Capability of $LiFePO_4$ by a New Highly Graphitic Carbon-Coating Method, *Acs Appl. Mater. Interfaces* **2016**, *8*, 15225-15231.

(16) Holtstiege, F.; Schmuch, R.; Winter, M.; Brunklaus, G.; Placke, T. New insights into pre-lithiation kinetics of graphite anodes via nuclear magnetic resonance spectroscopy, *J. Power Sources* **2018**, *378*, 522-526.

(17) Campéon, B. D. L.; Yoshikawa, Y.; Teranishi, T.; Nishina, Y. Sophisticated rGO synthesis and pre-lithiation unlocking full-cell lithium-ion battery high-rate performances, *Electrochim. Acta* **2020**, *363*, 137257.

(18) Toby, B. H. EXPGUI, a graphical user interface for GSAS, *J. Appl. Crystallogr.* **2001**, *34*, 210-213.

(19) Larson, A.; Von Dreele, R. Generalized structure analysis system (GSAS), *Alamos National Laboratory Report LAUR* **2004**, *96*, 748.

(20) Newville, M. IFEFFIT: interactive XAFS analysis and FEFF fitting, *J. Synchrotron Radiat.* **2001**, *8*, 322-324.

(21) Yabuuchi, N.; Takeuchi, M.; Komaba, S.; Ichikawa, S.; Ozaki, T.; Inamasu, T. Synthesis and electrochemical properties of $Li_{1.3}Nb_{0.3}V_{0.4}O$ as a positive electrode material for rechargeable lithium batteries, *Chem. Commun.* **2016**, *52*, 2051-2054.

(22) Yabuuchi, N.; Kim, Y.-T.; Li, H. H.; Shao-Horn, Y. Thermal Instability of Cycled LixNi0.5Mn0.5O2 Electrodes: An in Situ Synchrotron X-ray Powder Diffraction Study, *Chem. Mater.* **2008**, *20*, 4936-4951.

(23) De Picciotto, L.; Thackeray, M.; David, W.; Bruce, P.; Goodenough, J. Structural characterization of delithiated $LiVO_2$, *Mater. Res. Bull.* **1984**, *19*, 1497-1506.

(24) Sato, T.; Sato, K.; Zhao, W.; Kajiya, Y.; Yabuuchi, N. Metastable and nanosize cation-disordered rocksalt-type oxides: revisit of stoichiometric $LiMnO_2$ and $NaMnO_2$, *J. Mater. Chem. A* **2018**, *6*, 13943-13951.

(25) Wang, J.; Sun, X. Understanding and recent development of carbon coating on $LiFePO_4$ cathode materials for lithium-ion batteries, *Energy Environ. Sci.* **2012**, *5*, 5163-5185.

(26) de Picciotto, L. A.; Thackeray, M. M.; David, W. I. F.; Bruce, P. G.; Goodenough, J. B. Structural characterization of delithiated LiVO2, *Mater. Res. Bull.* **1984**, *19*, 1497-1506.

(27) Ji, H.; Urban, A.; Kitchaev, D. A.; Kwon, D.-H.; Artrith, N.; Ophus, C.; Huang, W.; Cai, Z.; Shi, T.; Kim, J. C.; Kim, H.; Ceder, G. Hidden structural and chemical order controls lithium transport in cation-disordered oxides for rechargeable batteries, *Nat. Commun.* **2019**, *10*, 592.

(28) Nien, Y.-H.; Carey, J. R.; Chen, J.-S. Physical and electrochemical properties of $LiFePO_4$/C composite cathode prepared from various polymer-containing precursors, *J. Power Sources* **2009**, *193*, 822-827.

(29) Tanaka, S.; Narutomi, T.; Suzuki, S.; Nakao, A.; Oji, H.; Yabuuchi, N. Acrylonitrile-grafted poly(vinyl alcohol) copolymer as effective binder for high-voltage spinel positive electrode, *J. Power Sources* **2017**, *358*, 121-127.

(30) Shimizu, S.; Rajendra, H. B.; Watanuki, R.; Yabuuchi, N. Li/Na Storage Properties of Disordered Carbons Synthesized by Mechanical Milling, *Electrochemistry* **2019**, *87*, 276-280.

(31) De Picciotto, L.; Thackeray, M.; Pistoia, G. An electrochemical study of the systems $Li_{1\pm x}V_2O_4$

and $Li_{1-x}VO_2$ ($0 \leqslant x \leqslant 1$), *Solid State Ion.* **1988**, *28*, 1364-1370.

(32) Baur, C.; Lăcătuşu, M.-E.; Fichtner, M.; Johnsen, R. E. Insights into Structural Transformations in the Local Structure of Li2VO2F Using Operando X-ray Diffraction and Total Scattering: Amorphization and Recrystallization, *ACS Appl. Mater. Interfaces* **2020**, *12*, 27010-27016.

(33) Yamamoto, T. Assignment of pre-edge peaks in K-edge x-ray absorption spectra of 3d transition metal compounds: electric dipole or quadrupole?, *X-Ray Spectrom.* **2008**, *37*, 572-584.

(34) Dahn, J.; Fuller, E.; Obrovac, M.; Von Sacken, U. Thermal stability of Li_xCoO_2, Li_xNiO_2 and λ-MnO_2 and consequences for the safety of Li-ion cells, *Solid State Ion.* **1994**, *69*, 265-270.

(35) Ji, H.; Urban, A.; Kitchaev, D. A.; Kwon, D. H.; Artrith, N.; Ophus, C.; Huang, W.; Cai, Z.; Shi, T.; Kim, J. C.; Kim, H.; Ceder, G. Hidden structural and chemical order controls lithium transport in cation-disordered oxides for rechargeable batteries, *Nat. Commun.* **2019**, *10*, 592.

(36) Lee, J.; Kitchaev, D. A.; Kwon, D. H.; Lee, C. W.; Papp, J. K.; Liu, Y. S.; Lun, Z.; Clement, R. J.; Shi, T.; McCloskey, B. D.; Guo, J.; Balasubramanian, M.; Ceder, G. Reversible Mn(2+)/Mn(4+) double redox in lithium-excess cathode materials, *Nature* **2018**, *556*, 185-190.

(37) Fan, X.; Ou, X.; Zhao, W.; Liu, Y.; Zhang, B.; Zhang, J.; Zou, L.; Seidl, L.; Li, Y.; Hu, G.; Battaglia, C.; Yang, Y. In situ inorganic conductive network formation in high-voltage single-crystal Ni-rich cathodes, *Nat. Commun.* **2021**, *12*, 5320.

(38) Wang, R.; Chen, X.; Huang, Z.; Yang, J.; Liu, F.; Chu, M.; Liu, T.; Wang, C.; Zhu, W.; Li, S.; Li, S.; Zheng, J.; Chen, J.; He, L.; Jin, L.; Pan, F.; Xiao, Y. Twin boundary defect engineering improves lithium-ion diffusion for fast-charging spinel cathode materials, *Nat. Commun.* **2021**, *12*, 3085.

(39) Kong, W.; Zhang, J.; Wong, D.; Yang, W.; Yang, J.; Schulz, C.; Liu, X. Tailoring Co3d and O2p Band Centers to Inhibit Oxygen Escape for Stable 4.6 V $LiCoO_2$ Cathodes, *Angew. Chem., Int. Ed.* **2021**, *133*, 2-13.

(40) Cai, Z.; Ji, H.; Ha, Y.; Liu, J.; Kwon, D.-H.; Zhang, Y.; Urban, A.; Foley, E. E.; Giovine, R.; Kim, H.; Lun, Z.; Huang, T.-Y.; Zeng, G.; Chen, Y.; Wang, J.; McCloskey, B. D.; Balasubramanian, M.; Clément, R. J.; Yang, W.; Ceder, G. Realizing continuous cation order-to-disorder tuning in a class of high-energy spinel-type Li-ion cathodes, *Matter* **2021**, *4*, 3897-3916.

TOC

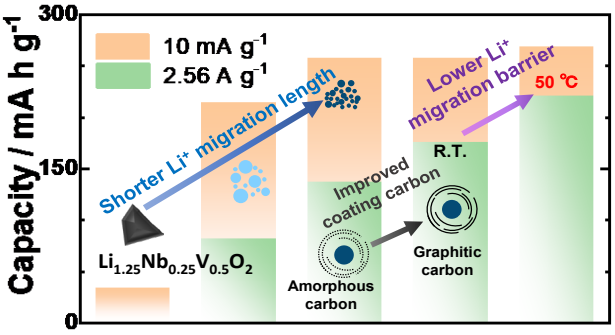
Capacity / mA h g-1
300
150
0
10 mA g-1
2.56 A g-1
Shorter Li+ migration length
Li1.25Nb0.25V0.5O2
Amorphous carbon
Improved coating carbon
Graphitic carbon
R.T.
Lower Li+ migration barrier
50 ℃